Available online at www.sciencedirect.com
ScienceDirect
Catalysis Today 130 (2008) 86–96
CATALYSIS TODAY
www.elsevier.com/locate/cattod

Recent STM, DFT and HAADF-STEM studies of sulfide-based hydrotreating catalysts: Insight into mechanistic, structural and particle size effects

F. Besenbacher [a], M. Brorson [b], B.S. Clausen [b], S. Helveg [b], B. Hinnemann [b], J. Kibsgaard [a], J.V. Lauritsen [a], P.G. Moses [c], J.K. Nørskov [c], H. Topsøe [b,*]

[a] *Department of Physics and Astronomy, Interdisciplinary Nanoscience Center (iNANO), University of Aarhus, DK-8000 Aarhus C, Denmark*
[b] *Haldor Topsøe A/S, Nymøllevej 55, DK-2800 Lyngby, Denmark*
[c] *Department of Physics and Center for Atomic-scale Materials Design (CAMD), NanoDTU, Technical University of Denmark, DK-2800 Lyngby, Denmark*

Available online 11 September 2007

Abstract

The present article will highlight some recent experimental and theoretical studies of both unpromoted MoS_2 and promoted Co–Mo–S and Ni–Mo–S nanostructures. Particular emphasis will be given to discussion of our scanning tunnelling microscopy (STM), density functional theory (DFT), and high-angle annular dark-field scanning transmission electron microscopy (HAADF-STEM) studies which have provided insight into the detailed atomic structure. In accordance with earlier theoretical studies, the experimental studies show that the Ni–Mo–S structures may in some instances differ from the Co–Mo–S analogues. In fact, the Co–Mo–S and Ni–Mo–S structures may be even more complex than previously anticipated, since completely new high index terminated structures have also been observed. New insight into the HDS mechanism has also been obtained and complete hydrogenation and hydrogenolysis pathways for thiophene hydrodesulfurization (HDS) have been calculated on the type of structures that prevail under reaction conditions. It is seen that important reaction steps may not involve vacancies, and special brim sites are seen to play an important role. Such studies have also provided insight into inhibition and support effects which play an important role in practical HDS. Recent STM studies have shown that MoS_2 clusters below 2–3 nm may exhibit new structural and electronic properties, and a large variety of size-dependent structures have been identified. In view of the large structure sensitivity of hydrotreating reactions this is expected to give rise to large effects on the catalysis.

Keywords: Hydrotreating; Hydrodesulfurization; Hydrodenitrogenation; HDS; Model catalyst; Scanning tunnelling microscopy; STM; Density functional theory; DFT; Molybdenum disulfide; MoS_2; Promoters; Morphology; Ni–Mo–S; Co–Mo–S; Inhibition; Thiophene; Pyridine; HAADF-STEM; Support interaction

1. Introduction

In recent years, new legislation regarding the sulfur content in transport fuels has resulted in the demand for ultra low sulfur diesel (ULSD), and this has introduced new challenges for hydrodesulfurization (HDS) in the refining industry [1–9]. In addition, the demand for diesel fuels is increasing, and as the availability of light petroleum resources decreases, increasingly heavy feedstocks have to be refined. In order to achieve the higher sulfur conversion, very refractory sulfur compounds, like dialkylated dibenzothiophenes (DBT), need to be removed [1,3–6,10]. It has been known for some time that the conversion of the sterically hindered DBTs mainly proceeds via a pre-hydrogenation route (HYD) rather than the direct desulfurization route (DDS), which dominates for molecules like DBT [3]. However, under industrial conditions, the presence of other compounds in the feed often changes the relative role of the HYD and the DDS pathways. In particular, specific basic nitrogen-containing compounds inhibit HDS, and these compounds are observed to mainly inhibit the HYD pathway [11–13]. Furthermore, H_2S is an HDS inhibitor, and interestingly, it mainly inhibits the DDS rather than the HYD pathway [1]. To improve HDS catalysts and gear them to the increasingly heavy feedstocks, detailed understanding of their

* Corresponding author.
E-mail address: het@topsoe.dk (H. Topsøe).

0920-5861/$ – see front matter © 2007 Published by Elsevier B.V.
doi:10.1016/j.cattod.2007.08.009

mechanistic action is necessary so that targeted modifications can be made.

In order to elucidate the HDS reaction and the two different HYD and DDS pathways in detail, it is important to characterize the active nanostructures and in particular to identify the active sites for the two pathways. Until the early 1980s, very little information was available on the structure of active hydrotreating catalysts. A key discovery was the identification of the MoS_2 and Co–Mo–S structures by EXAFS, Mössbauer and infrared techniques, and it was shown that the Co–Mo–S structure was responsible for the promotion of catalytic activity [14–18]. These results revealed that Co–Mo–S (and also Ni–Mo–S) structures are small MoS_2-like nanocrystals, where the promoter atoms are located at the edges of the MoS_2 layers. The results furthermore suggested that Co atoms are located in the same plane as Mo, but that their local coordination is different. In spite of the significant progress, it was for a long-time difficult to address the issue of the detailed edge structure of unpromoted and promoted MoS_2, as no atomic-resolved structures could be obtained. As a consequence, it has also been difficult to understand the nature of HYD and DDS pathways and sites. Recently, we have achieved a large breakthrough in the structural studies of the active nanostructures in HDS using scanning tunnelling microscopy (STM) to image the real-space structure of MoS_2 nanoclusters grown on flat model substrates. With the STM, it was possible for the first time to reveal the equilibrium morphology of the nanoclusters. Furthermore, atomic-resolution STM images made it possible to elucidate the detailed structure of the catalytically important edges, the sulfur coverage and the location of sulfur vacancies, which are normally considered to be active sites [19]. In further studies, we have also managed to synthesize and characterize the atomic-scale structure of Co–Mo–S and Ni–Mo–S and thereby it has been possible to obtain information on the location of the Co and Ni promoter atoms [20,21]. Recently, MoS_2, WS_2 and promoted structures were studied by another new technique, high-angle annular dark-field scanning tunnelling electron microscopy (HAADF-STEM), and additional information on the morphology of MoS_2- and WS_2-based nanostructures could be obtained [22–24]. In most of the STM studies, gold was used as a support of the sulfide nanostructures. Since gold is a weakly interacting support, the studies have provided important insight into the intrinsic properties of the nanostructures. In industrial HDS catalysts, the support usually plays a significant role and the STM studies have recently been extended to carbon-supported systems [25]. Many earlier studies have indicated that hydrotreating reactions are extremely sensitive structure [1]. One may therefore expect that the reactions will depend strongly on the particle size, but not much has been known about such effects. Recently, STM has for the first time provided us with atom resolved images of MoS_2 clusters of different sizes [26]. Many size-dependent structural and electronic changes were observed and such effects must clearly also be taken into account when addressing the catalysis.

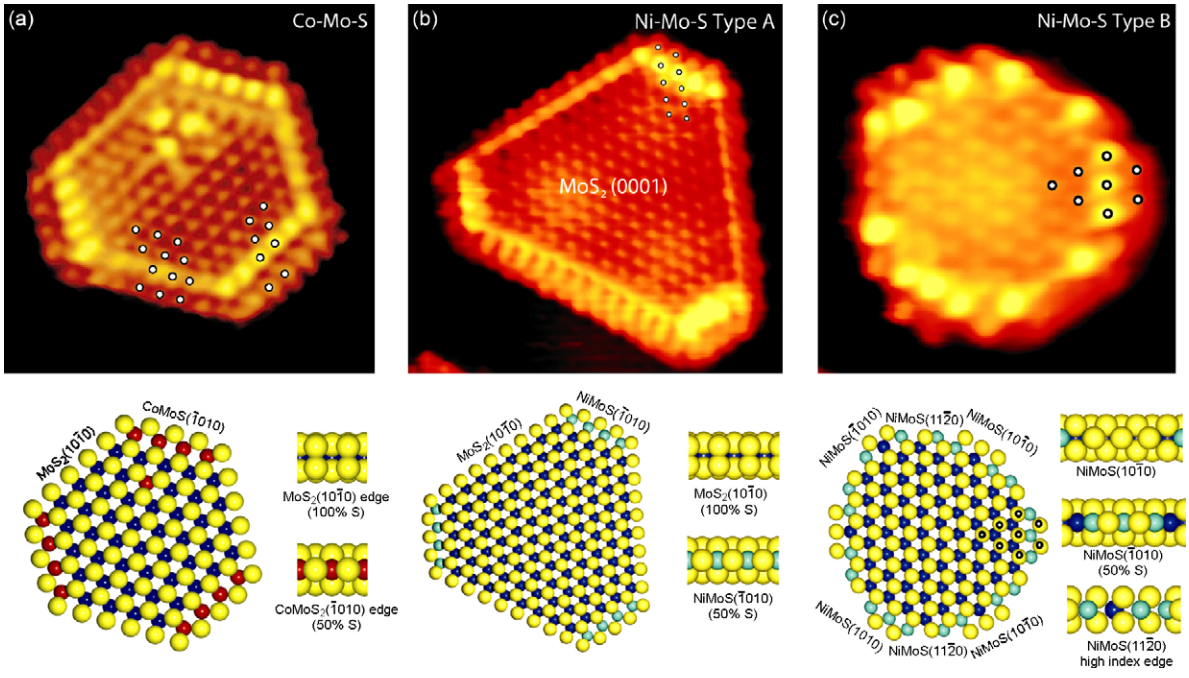

Fig. 1. (a) Top: Atom-resolved STM image (51 Å × 52 Å, I_t = 0.81 nA and V_t = −95.2 mV) of a hexagonally truncated Co–Mo–S nanocluster supported on Au(1 1 1). The superimposed white dots illustrate the registry of protrusions on both types of edges. Bottom: A ball model (top and side views, respectively) of the Co–Mo–S nanocluster based on DFT calculations. (b) Top: Atom-resolved STM image (61 Å × 61 Å, I_t = 0.51 nA and V_t = −600 mV) of a hexagonally truncated type A Ni–Mo–S nanocluster supported on Au(1 1 1). Bottom: A ball model (top and side views, respectively) of the Ni–Mo–S type A nanocluster based on DFT calculations. (c) Top: Atom-resolved STM image (39 Å × 40 Å, I_t = 0.44 nA and V_t = −520 mV) dodecagonally shaped type B Ni–Mo–S nanocluster supported on Au(1 1 1). Bottom: A ball model (top and side views, respectively) of the Ni–Mo–S type B nanocluster based on DFT calculations. (Mo: blue; S: yellow; Co: red; Ni: cyan). Adapted from [21]. (For interpretation of the references to colour in this figure legend, the reader is referred to the web version of the article.)

First principles modelling techniques, like density functional theory (DFT), have over the last decade provided increasing insight into atomic structure and reactivity of the active phases of HDS catalysts. DFT can often provide information that is complementary to the multitude of experimental information, and the synergy of theoretical and experimental approaches can thus give a very detailed picture of catalyst structure and reactivity. After our initial studies of Co–Mo–S [27–29], we have recently used this approach in a series of studies, where STM and DFT were combined to obtain insight into the structure of unpromoted and promoted MoS_2 under different conditions [30–33,21]. The general approach of combining DFT with the chemical potential of the gas phase can be used to connect DFT calculations performed at 0 K and in vacuum to reaction conditions with relevant temperatures and pressures [34–39].

The very powerful combination of STM experiment and DFT calculations has led to several important findings in our studies, and one of the most significant results was the discovery of the so-called brim states and their role in HDS catalysis. It was found that the Mo edge exhibits a special electronic edge state, which can easily be identified in STM images of the nanoclusters as a very bright brim extending along the edges (see e.g. Fig. 1). These brim states arise from a perturbation of the electronic structure near the edges relative to the interior part of the clusters. Detailed analysis using DFT revealed the presence of edge states, which are metallic states that are localized at the cluster edges and give rise to the brim states [30]. Quite surprisingly, it was observed that these states possess reactivity towards the hydrogenation of thiophene, which could be observed using STM [31,32]. Thus, insight into these sites is essential for understanding hydrotreating reactions.

The ever increasing computational power makes it possible to study increasingly complex systems, and in recent years a number of reports on catalyst-support interactions have been published [40–44]. Also, the reaction pathway of thiophene and thiophene derivatives on MoS_2 have been studied by us [45] and several other groups [46–49] and thus, we can begin to understand reaction pathways and find descriptors for catalytic activity.

In this review, we will highlight some of the above-mentioned developments. In Section 2, we discuss the recent STM and DFT studies of promoted CoMoS and NiMoS structures as well as HAADF-STEM studies on unpromoted and promoted MoS_2 and WS_2. In Section 3, we summarize the results concerning support interactions and in Section 4 we discuss recent developments concerning reaction pathways and inhibition. In Section 5, recent STM results regarding size effects are described.

2. Structure of MoS_2, Co–Mo–S and Ni–Mo–S

According to the now well-accepted Co–Mo–S model for the promoted MoS_2 hydrotreating catalysts, the Co and Ni promoter atoms are located at edge positions of MoS_2 nanostructures. Their substitution of Mo at edge sites is believed to enhance vacancy formation and the creation of new and more active sites. Several studies have been carried out to correlate the structure of the active promoted phases to the activity [1,15,17], but the exact location and coordination of the promoter atoms have been debated extensively [1,14,50–54]. Lack of structural insight has hampered the progress. Consequently, the origin of the promoting effect of Co and Ni is still not fully understood, and in particular it has been interesting to resolve the origin of the different specific selectivities with respect to hydrodesulfurization (HDS), hydrodenitrogenation (HDN) and hydrogenation (HYD) for the two types of promoted systems [1,3,4,8,10,55].

Following the initial STM studies of unpromoted MoS_2 nanoclusters [19], we have used STM to reveal the atomic scale structure of both Co–Mo–S [20] and more recently Ni–Mo–S [21]. Fig. 1 shows the STM images of Co–Mo–S and Ni–Mo–S nanoclusters. One can see that the main indicator of the formation of promoted Co–Mo–S and Ni–Mo–S phases is a distinct change in morphology compared to the unpromoted MoS_2 nanoclusters, which under similar synthesis conditions have a very regular triangular shape. This change in morphology is concluded to be mainly driven by the preference for the promoter atoms (Co and Ni) to substitute certain sites. In many instances, there is a preference for the substitution at the $(\bar{1}\,0\,1\,0)$ S edges of MoS_2 rather than at the $(1\,0\,\bar{1}\,0)$ Mo edges which under similar conditions are the only edges exposed in the unpromoted triangular clusters.

The above situation is illustrated for Co–Mo–S in Fig. 1a, which shows that the nanocluster adopts a clear hexagonally truncated shape, indicating that both $(1\,0\,\bar{1}\,0)$ Mo edges and $(\bar{1}\,0\,1\,0)$ S edges are present. One type of edge in the Co–Mo–S structure is found to be identical to that observed for the unpromoted MoS_2 triangles [19], with the outermost row of protrusions out of registry with the basal plane S atoms and a clear bright brim along the edge. This type of edge can therefore be identified as a $(1\,0\,\bar{1}\,0)$ Mo edge. The other edges must according to the symmetry be the $(\bar{1}\,0\,1\,0)$ S edges. This type of edge is seen to exhibit an even brighter brim structure in which individual protrusions can be identified. The periodicity of one lattice distance along the brim indicates that Co atoms have replaced all Mo atoms at the S edge creating a $(\bar{1}\,0\,1\,0)$ Co–Mo–S edge. It is, however, not straightforward to identify the exact edge structure and sulfur termination exclusively from STM images. We have therefore performed DFT calculations to identify the edge termination of the $(\bar{1}\,0\,1\,0)$ Co–Mo–S edges [21], and simulated STM images show that only a 50% sulfur covered edge is consistent with the experimental STM images. Furthermore, this theoretical analysis reveals that a metallic edge state (brim state) is responsible for the very bright brim observed at the promoted edge. This resulting local structure around the Co atoms is in good agreement with previous spectroscopic measurements [51,56,57].

The edge truncation effects observed in the STM studies are more complex for the Ni–Mo–S nanoclusters [21]. In addition, the nature of the truncation for the Ni–Mo–S system was seen to depend on the cluster size. The larger type A clusters are characterized by a hexagonally truncated shape similar to that

of the Co–Mo–S nanoclusters (See Fig. 1b). The smaller type B clusters, on the other hand, have a more complex dodecagonal morphology (See Fig. 1). The Ni–Mo–S type A structures are terminated by two types of edges. As for the Co–Mo–S case, the Ni–Mo–S type A clusters expose both an unpromoted $(1\,0\,\bar{1}\,0)$ Mo edge and a new $(\bar{1}\,0\,1\,0)$ Ni–Mo–S edge structure, in which Ni has fully substituted all edge Mo sites. In order to understand the structure and properties of this edge in detail, we have again used DFT. The DFT-based simulated STM images show that only an edge with 50% sulfur coverage is energetically favourable and consistent with the experimental images. The structure of Ni–Mo–S type A, which is depicted in the ball model in Fig. 1b, is thus similar to that of Co–Mo–S. The DFT calculations of the $(\bar{1}\,0\,1\,0)$ Ni–Mo–S edge show that the bright brim observed with STM is related to two distinct Ni–Mo–S metallic edge states. One of the metallic Ni–Mo–S edge states is similar to the one in Co–Mo–S, but the other one has no MoS_2 or Co–Mo–S counterpart [21,30] and it is possible that this edge state plays a catalytic role and is responsible for differences in catalytic activity and selectivity between Co–Mo–S and Ni–Mo–S. The smaller dodecagonally shaped type B Ni–Mo–S clusters (Fig. 1c) are structurally more complicated and are seen to be terminated by three different types of edges. Two of the edge types can be identified as the same fundamental types as the $(1\,0\,\bar{1}\,0)$ Mo edge and the $(\bar{1}\,0\,1\,0)$ Ni–Mo–S edge also found in the type A Ni–Mo–S clusters. However, the STM images show bright protrusions on the Mo edges indicating that Ni atoms also have substituted at Mo edge sites creating $(1\,0\,\bar{1}\,0)$ Ni–Mo–S edges (Fig. 1c). Comparing the experimental STM images with simulated STM images from DFT, we conclude that type B $(1\,0\,\bar{1}\,0)$ Ni–Mo–S edges have a partial substitution of Mo by Ni, and only the parts of the edge with alternating Mo–Ni sections are seen to have sulfur adsorbed [21]. The last type of edge present in type B Ni–Mo–S is associated with a high-index $(1\,1\,\bar{2}\,0)$ edge. The presence of such edges is quite surprising, since previously, such edges have not been considered as stable edge terminations in Co–Mo–S or Ni–Mo–S structures. The STM experiments and the HAADF-STEM measurements discussed below are the first experimental evidence that such edges may be present under sulfiding conditions.

The presented observations suggest that the promoting role of Co and Ni may be two-fold. The change in the electronic structure as indicated by the modified brim and the lower S coordination on the promoted $(\bar{1}\,0\,1\,0)$ Ni–Mo–S edges may be an attractive situation enabling adsorption of sulfur-containing molecules. Furthermore, the presence of Ni–Mo–S type B clusters clearly demonstrate that there may be major differences in the morphologies of Co–Mo–S and Ni–Mo–S catalysts exposed to similar sulfiding environments, and this may be a key to explain the different selectivities of the two systems in the hydrotreating processes.

Recently, we have employed high-angle annular dark-field scanning transmission electron miscroscopy (HAADF-STEM) to obtain morphological information on unpromoted and promoted WS_2 and MoS_2 structures and to gain more insight into the changes induced by the promoter atoms [22–24]. Traditionally, researchers have been using high-resolution transmission electron microscopy (HRTEM) to obtain morphological insight into HDS catalysts [58–72]. However, it has been difficult to get such insights from HRTEM measurements since single S–Mo–S layers are typically only imaged when they are oriented approximately edge-on relative to the electron beam, i.e. the layers are viewed as lines in the images. In contrast, HAADF-STEM uses electron scattering at high angles to create a *Z*-contrast image with *Z* denoting the atomic number. This situation is especially advantageous for heavy elements and in the first study [22], we investigated WS_2/C catalysts and observed that even single WS_2 layers could be imaged with the beam along the *c*-axis. In this way, the morphology of the layers could be directly imaged. In accordance with the STM results, we observed that the shape of the nanostructures may deviate significantly from the hexagonal morphology observed for bulk crystals. Recently, we have applied this method to MoS_2, Co–Mo–S and Ni–Mo–S structures [24] and some of the resulting HAADF-STEM pictures are shown in Fig. 2. It can be seen that in spite of the high sulfiding temperature (1073 K), many of the single layer clusters still contain irregularities and defects, which distinguish them from the much more regular STM images of MoS_2 on Au(1 1 1). Also in industrial catalysts, the structures may have defects and layers are often curved [1]. It should be remarked that the clusters observed here are larger

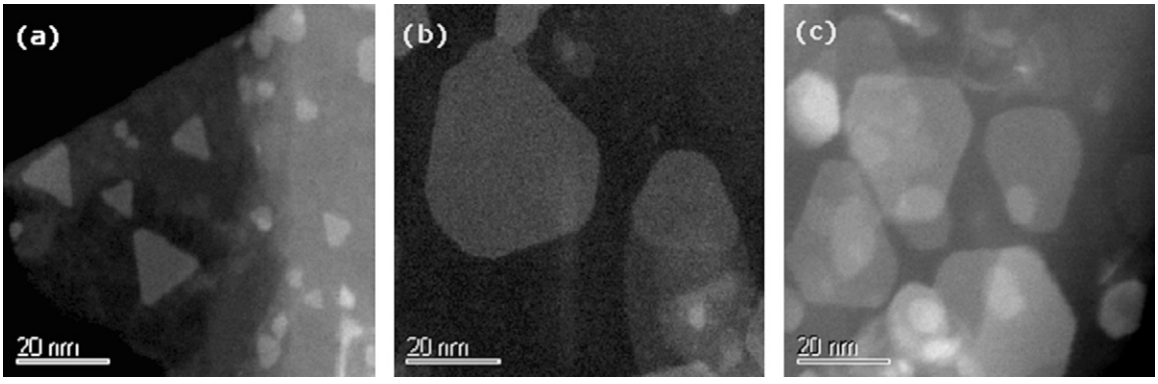

Fig. 2. HAADF-STEM images of (a) MoS_2, (b) Co–Mo–S and (c) Ni–Mo–S clusters supported on a thin graphite sheet oriented approximately perpendicular to the line of observation. The image (c) displays accidental overlap of clusters located along the same line of observation, possibly clusters located at opposite sides of the same graphite sheet. Adapted from Ref. [24].

than the ones in the STM study on Au(1 1 1). We find that most of the imaged clusters are single-layer clusters, as also shown by edge-on images presented in [22]. For the unpromoted MoS_2 structures, we find that the predominant shape is a truncated hexagon. From comparison with the STM images of MoS_2 on Au(1 1 1) [19] and with DFT calculations on edge stability [38], one can assume that predominantly Mo edges are exposed and they therefore correspond to the longer edges observed in the images. The promoted Co–Mo–S and Ni–Mo–S structures were also investigated and they are depicted in Fig. 2b and c, respectively. In accordance with the STM results it is found that promotion changes the morphology of the nanoclusters and that their shape becomes significantly more hexagonal. Furthermore, some of the hexagons appear with rounded corners, which indicate that high-index edge terminations are exposed also in the case of Co–Mo–S. These results differ from the Co–Mo–S and Ni–Mo–S structures on Au(1 1 1) studied by STM [21], where only Ni–Mo–S was observed to expose higher-index edge terminations. This difference may be due to the different supports as well as different preparation and sulfidation methods. The STM samples have been prepared by gas phase metal deposition onto a gold surface, whereas the HAADF-STEM samples have been prepared by impregnation of carbon powder followed by sulfidation. It is not surprising that the choice of such methods may greatly influence the structure of the catalyst [1]. However, considering the different synthesis methods and supports, it should be emphasized that many of the observed structure and the morphology changes induced by Co and Ni in the STM and HAADF-STEM experiments are rather similar. Regarding the possible role of the support, it should be noted that we recently have studied MoS_2 structures on graphite by STM [25], and these results are discussed in the following section.

3. Support interactions

The role of support interactions has been an important topic in catalysis research for many years, since the catalytic properties of MoS_2 are significantly influenced by the support [1]. The most common support is high-surface area alumina, since it allows for the production of small stable nanoclusters of MoS_2. Preparation conditions influence the activity significantly, e.g. it has been observed that an increase in sulfidation temperature resulted in the formation of modified Co–Mo–S structures [73], which had a significantly higher activity than those prepared at lower temperatures. These structures were termed Type II Co–Mo–S as opposed to the Type I Co–Mo–S structures formed at lower temperatures. Extensive characterization studies using EXAFS, FTIR and a multitude of other techniques [74–78] have suggested that Type I Co–Mo–S structures contain Mo–O–Al linkages with the support, whereas no such linkages are present in Type II structures. The Co promoter atoms are not involved in the formation of these linkages, as could be shown by Mössbauer spectroscopy [79,80]. Many studies have shown that catalysts with Type II structures often contain multilayer Co–Mo–S nanoclusters. In this case, only the layers close to the support may be bound to the latter by linkages, whereas the other layers only interact weakly by van der Waals forces and thus exhibit Type II-like activity. One way to avoid the Type I linkages is to increase the sulfidation temperature, but this has a number of unwanted side effects, e.g. sintering and loss of surface area. A different approach is to avoid the formation of linkages altogether and form directly Type II structures, and several studies have shown that this indeed is possible e.g. by the use of chelating ligands or additives [80–82]. It has also been shown that Type II structures may dominate when employing weakly interacting supports as e.g. carbon [1].

Table 1
The investigated structures for the position of oxygen linkages and the corresponding energies (in kJ/mol) for the creation of linkages

Position of OH group	Linkages every row (kJ/mol)	Linkages every sec. row (kJ/mol)
Outer row at Mo edge	0	0
Second row at Mo edge	89	25
Second row at S edge	52	7
Outer row at S edge	−152	−63

Linkages at the outer row of the Mo-edge are taken as the reference energy. Adapted from Ref. [42].

It is of significant interest to understand these support effects in detail, and theoretical modelling with density functional theory has been of great use to investigate these aspects. A few earlier [40,41] and several recent studies [43,44] have investigated support effects by modelling promoted and unpromoted MoS_2-based cluster structures on different facets of γ-Al_2O_3, and in the latter studies different adsorption geometries and configurations were mapped out in great detail. Such investigations are complicated further by the fact that the precise location of non-spinel sites in γ-Al_2O_3 is not completely known and still under discussion [83–87].

In a recent study [42], we have investigated a simplified system, where we modelled the linkages by hydroxyl groups,

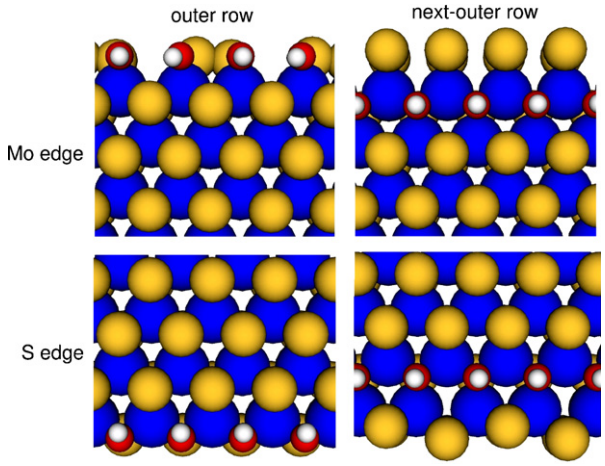

Fig. 3. The investigated structures for the position of oxygen linkages. The corresponding energies are listed in Table 1. Color code of the atoms: sulfur (yellow), molybdenum (blue), oxygen (red), hydrogen (white). Adapted from Ref. [42]. (For interpretation of the references to colour in this figure legend, the reader is referred to the web version of the article.)

concentrating exclusively on the chemical impact of support linkages without considering steric issues. We found that linkages have a thermodynamic preference for the S-edge, as illustrated in Table 1 and Fig. 3. Furthermore, vacancy formation, both at the linkage sites themselves and in the immediate vicinity, is energetically much more expensive and therefore not favoured. We also found that the electronic structure of the linkage sites as well as hydrogen adsorption differs significantly from that of the S-edge without linkages. These findings could explain several experimental observations: In previous high temperature sulfidation studies [16,79] it was found that the temperature at which the support linkages can be broken, i.e., the Type I to Type II transition temperature, depends on the Co loading. For low Co content, the Type I to Type II transition takes place at a higher temperature than for high Co content, and for unpromoted MoS_2, the transition was not observed at all in the employed temperature region. Combining our results with the results that Co primarily is located at the S-edge (see previous section), these results are easy to understand: Linkages and Co are likely not located at the same site, and therefore at high Co content (or higher coverage of the S-edge by Co), there are fewer linkages that have to be broken and thus the transition temperature is lower. In some systems, the transition occurred at the temperature at which edge saturation had occurred. This simplified support interaction model thus allowed us to gain some insight into important phenomena which had remained unexplained for two decades. The results also showed that the linkages may also significantly influence the brim sites which play an important role in the catalysis (see Section 4).

The choice of substrate can be, as discussed above, used as a means of influencing catalyst structure and properties, and in this regard, graphite is highly interesting since Type II structures are formed [88] and indeed, carbon-supported MoS_2-based hydrotreating catalysts exhibit a very high HDS reactivity [88,18,89,90]. This motivation has recently led us to apply STM to investigate the atomic-scale structure and morphology of MoS_2 nanoclusters synthesized on a graphite (HOPG) substrate [25]. Due to a very weak bonding and high mobility of Mo to the graphite it was not possible to synthesize highly dispersed MoS_2 clusters on the clean single crystal HOPG surface. Instead, a HOPG substrate, pretreated by ion bombardment, was used since this created a low density of surface defects capable of stabilizing well-dispersed nanoclusters. Not surprisingly, both the crystallinity, morphology, and stacking of the MoS_2 nanostructures were found to be dependent on the subsequent annealing temperature. Clusters synthesized at 1000 K consist predominantly of a single S–Mo–S layer, whereas the clusters synthesized at 1200 K exclusively grow as stacked multilayer clusters containing typically 2–6 S–Mo–S layers. Atom-resolved STM images of both the single- and multilayer clusters reveal a well ordered MoS_2 basal plane structure in the interior consisting of hexagonally arranged protrusions with an average interatomic spacing of 3.15 Å, in perfect agreement with the interatomic spacing of the S atoms in the (0 0 0 1) basal plane of bulk MoS_2.

The preferential shape of small single-layer MoS_2 nanoclusters is observed to be hexagonal (see Fig. 4). However, the morphology of large single-layer clusters is significantly more complex due to pinning of the cluster edges to defects. Such effects were also observed by HAADF-STEM [22–24]. The interface structure between the S–Mo–S layer and the HOPG is obtained in atomic detail in the STM images of the single-layer clusters. In this way it was possible to pinpoint the anchoring sites of the MoS_2 nanoclusters as surface defects preferentially located directly underneath the nanoclusters edges and not the basal plane.

The multilayer clusters are also predominantly shaped as hexagons (See Fig. 4b). This is not surprising since adjacent layers, in the 2H stacking commonly encountered in bulk MoS_2, are translated and rotated 60° around the *c*-axis. The result is that Mo atoms in one layer are placed on top of S atoms in the next layer and a multilayer cluster will therefore expose Mo edges and S edges in an alternation fashion, and any difference in edge free energy thus tends to cancel out.

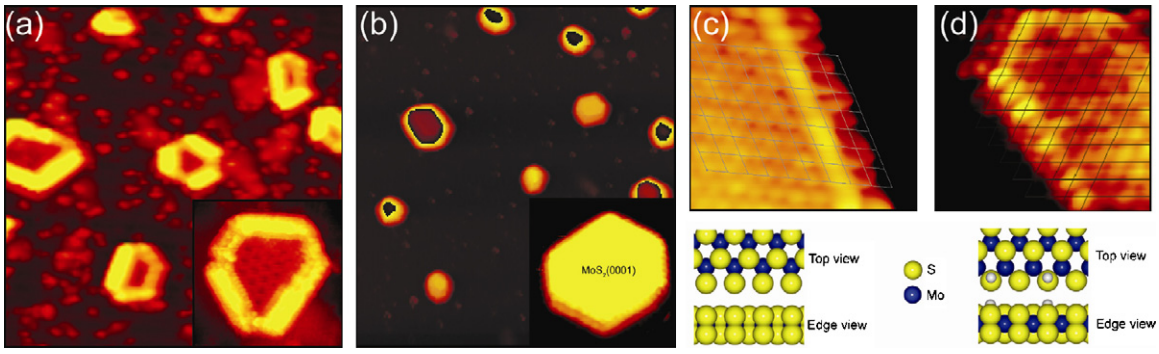

Fig. 4. (a) STM image (430 Å × 430 Å, I_t = 0.23 nA and V_t = −1250 mV) of single-layer MoS_2 nanoclusters on HOPG. The insert shows a zoom-in on a cluster (b) STM image (1000 Å × 1000 Å, I_t = 0.19 nA and V_t = −1250 mV) of multilayer MoS_2 nanoclusters on HOPG. The insert shows a zoom-in on a cluster clearly showing the hexagonal shape. (c) Top: Atom-resolved STM image (36 Å × 35 Å, I_t = 0.23 nA and V_t = −7.9 mV) showing the atomic-scale structure of the (1 0 $\bar{1}$ 0) Mo-edge on a multilayer cluster. The superimposed grid on the basal plane sulfur atoms shows that protrusions at the edge are out of registry. Bottom: A ball model (top and side view, respectively) of the Mo-edge fully saturated with sulfur dimers corresponding to the experiment. (d) Top: Atom-resolved STM image (41 Å × 37 Å, I_t = 0.19 nA and V_t = 0.6 mV) of the ($\bar{1}$ 0 1 0) S-edge. The grid shows that protrusions on the S-edge are imaged in registry. Bottom: A ball model of the fully sulfided S-edge and with a fractional coverage of S–H groups representing the experimental image of the S-edge (Mo: blue; S: yellow; H: gray). Adapted from Ref. [25]. (For interpretation of the references to colour in this figure legend, the reader is referred to the web version of the article.)

The top layer of the multilayer clusters is not perturbed by the defects in the HOPG and can thus be used to obtain interesting atom-resolved information. One of the two edge types has the outermost row of protrusions out of registry with the basal plane S atoms and a clear bright brim along the edge (Fig. 4c). This type of edge is thus completely identical to the edges observed for the unpromoted MoS_2 triangles [19] and this type of edge is therefore identified as a Mo edge fully saturated with sulfur dimers. Importantly, the atom-resolved STM images provide solid evidence for one-dimensional metallic brim sites on the graphite-supported MoS_2, which as discussed further in Section 4 play an important role in the catalytic properties of single-layer MoS_2 [31,32]. Thus the brim sites are not special for the gold supported systems but likely to be an important feature of all MoS_2- and WS_2-based catalysts on different supports.

The other type of edge must according to the symmetry be a S edge (Fig. 4d). This type of edge was not previously observed under the same sulfiding conditions for the Au supported system, since only Mo edges are exposed for the single layer MoS_2 triangles under such conditions [19]. However, the appearance of the edge with the outermost row of protrusions in registry with the basal plane S atom and clearly resolved protrusions along the brim resembles the S edges imaged for hexagonal MoS_2 clusters synthesized in a mixture of H_2 and H_2S [33]. The S edges formed under these conditions are fully sulfided with hydrogen adsorbed in the form of S–H groups [34,38,91,33]. The similarities suggest that the multilayer clusters also expose this kind of S edges and it thus seems plausible that the intensity variation observed along the brim (Fig. 2d) is due to a partial hydrogen adsorption. The observation of hydrogen adsorbates at the clusters edges is highly interesting from a catalytic point of view, since both adsorption of the S-containing molecule and dissociation of H_2 are required to facilitate the HDS reaction, as will be discussed further in the following section.

4. Hydrogenation and direct desulfurization reaction routes

As discussed in Section 2, STM images have clearly revealed that MoS_2, Co–Mo–S, and Ni–Mo–S expose bright brims at the edges [19,20,21]. Using DFT, these brims have been shown to be the result of one or more metallic edge states [30,38]. Combined STM and DFT studies have investigated thiophene HDS over MoS_2 particles at STM conditions, and it was found that fully sulfided MoS_2 particles which have a bright brim are able to hydrogenate thiophene and make 2,5-dihydrothiophene. Furthermore, it is important to note that at these sites one is also able to break one S–C bond and thereby produce *cis*-2-butenethiolate [31,32]. These studies indicate that brims can play a role in hydrogenation reactions and also in S–C scission reactions. Contrary to the general view in the previous literature, the results show that S–C scission may occur without the involvement of vacancies.

In a recent DFT study [45], we have further investigated the HDS reactions of thiophene over MoS_2. In order to make the studies of direct relevance for actual HDS, we have as starting point used the edge configurations corresponding to actual HDS conditions. The study clearly shows that there may be several HYD and DDS pathways on the $(1\,0\,\bar{1}\,0)$ Mo and the $(\bar{1}\,0\,10)$ S edges. The structure of MoS_2 is very dependent on reaction conditions [34–39] and the structure at HDS conditions (seen in Fig. 5) may therefore be quite different from that present at vacuum conditions for STM imaging. However, it was found that the brim sites consisting of metallic edge states are also present at HDS conditions [38].

The reaction scheme obtained from our DFT study is depicted in Fig. 5. In general, we find that the active site at the S edge is most likely a vacancy site whereas the active site at the Mo edge is a brim site and not a coordinatively unsaturated site [45]. It is important to note that the brim sites are present at the equilibrium edge configuration under HDS conditions, while

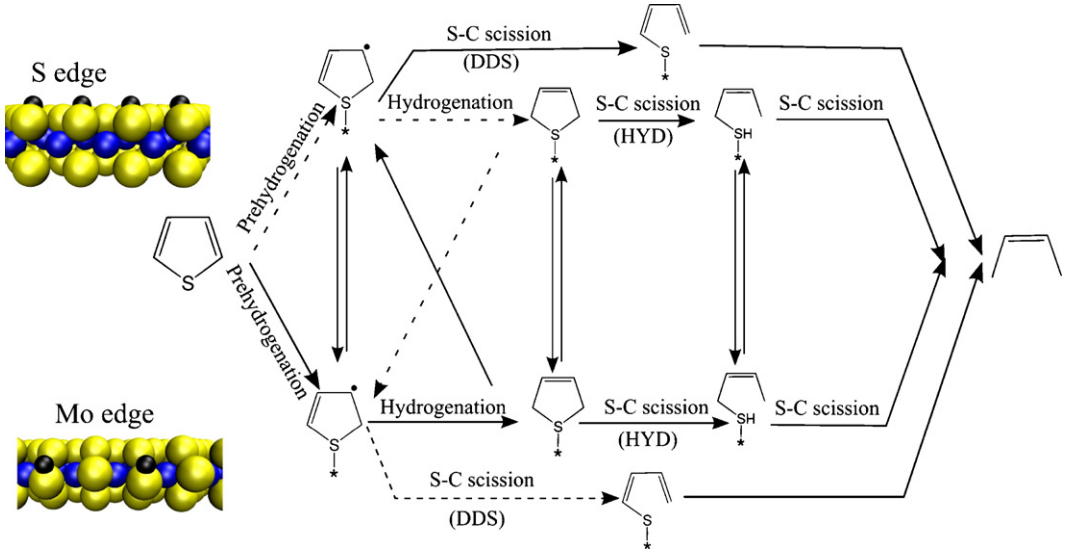

Fig. 5. Schematic overview of HDS of thiophene. Upper part: The equilibrium structure at HDS conditions at the S edge and the possible reactions occurring at the S edge. Lower part: The equilibrium structure at HDS conditions at the Mo edge and the possible reactions occurring at the Mo edge. The dotted lines represent slow reactions. Adapted from Ref. [45].

the S edge vacancy site first needs to be created from the equilibrium structure. For this creation of the vacancy site, it was found that the effective energy barrier for vacancy formation depends on the hydrogen pressure. Investigating the HYD pathway it was found that hydrogenation and H transfer steps have lower barriers at the Mo edge brim site than at the S edge vacancy sites. In contrast, the S–C scission reactions have lower barriers at the S edge. Furthermore, thiophene prefers to be adsorbed at the Mo edge while the intermediates prefer to adsorb at the S edge vacancy site.

The investigated HYD pathway proceeds via thiophene adsorption, followed by hydrogenation to 2-hydrothiophene, and further hydrogenation to 2,5-dihydrothiophene and then subsequent S–C scission. The DDS pathway is initiated by hydrogenation to 2-hydrothiophene which is then immediately followed by S–C scission. The relative importance of the S edge and the Mo edge in HDS of thiophene was found to depend on reaction conditions and the different possible reaction pathways have been summarized in Fig. 5. The HYD pathway may occur at the Mo edge brim site without involving a coordinative unsaturated site as seen in Fig. 5. Therefore, the Mo edge brim site is able to both hydrogenate thiophene and break S–C bonds. The HYD pathway may also proceed via prehydrogenation and hydrogenation at the Mo edge brim site, diffusion to the S edge and then S–C scission at the S edge vacancy site. The S–C scission reactions have lower barriers at the S edge and the intermediates bind more strongly but the number of active sites is much lower since vacancies need to be created prior to reaction. The edge interaction between the Mo edge and the S edge will probably be of importance at high hydrogen pressures or low H_2S pressures where the vacancy coverage at the S edge is significant. The S edge vacancy site was also found to be the primary site for the S–C scission in the DDS pathway. The crucial step is for both the HYD and the DDS pathway proposed to be the active site regeneration. It was therefore proposed that an activity descriptor could be the minimum energy required to either add or remove S from the equilibrium edge structures.

The identification of the Mo edge brim site as the hydrogenation site explains the low inhibiting effect of H_2S on hydrogenation as found in many studies [1,92], since H_2S does not bind to the fully coordinated brim sites. Inhibition of HDS by nitrogen-containing compounds is of central importance in practical HDS of many feedstocks [1,8,93]. In particular, it has been shown that basic heterocyclic compounds as e.g. pyridine primarily inhibit the HYD pathway of the HDS reaction [94,95]. This is especially important, as there is an increasing demand for deep desulfurization, where sterically hindered alkyl substituted molecules like 4,6-DMDBT have to be desulfurized. In these molecules, access to the sulfur is sterically hindered and HDS of the pure component proceeds primarily via the HYD route [3], and thus there is an interest to avoid inhibition of especially this route. Furthermore, understanding of inhibition, by e.g. pyridine, offers the opportunity to gain further insight into where the reactive sites are located. For non-sterically hindered heterocyclic compounds with nitrogen in a six-membered ring, as for instance pyridine, it has been observed that the inhibitor strength and the gas phase proton activities are correlated [12,96]. Aromatic hydrocarbons, e.g. benzene also primarily inhibit the HYD route, but their effect is much weaker than for e.g. pyridine.

In a recent study [97], we investigated the effects of the three different inhibitors pyridine, benzene and H_2S. We found that pyridine itself only adsorbs weakly on the Mo edge, but in the presence of hydrogen under HDS conditions, pyridine becomes protonated. The resulting pyridinium ion adsorbs strongly on the Mo-edge and forms a chemical bond to the surface, as shown in Fig. 6. It should be noted that the pyridinium ion interacts with the special brim sites that, as discussed above, also are involved in the HYD reaction [30]. Interestingly, it was found that protonation of pyridine does not take place at the S edge, as hydrogen itself is too strongly bound to this edge and thus not available. Benzene and H_2S only bind weakly to both edges, which explains why their inhibition effect is much lower than pyridine. These results also point to the Mo edge primarily

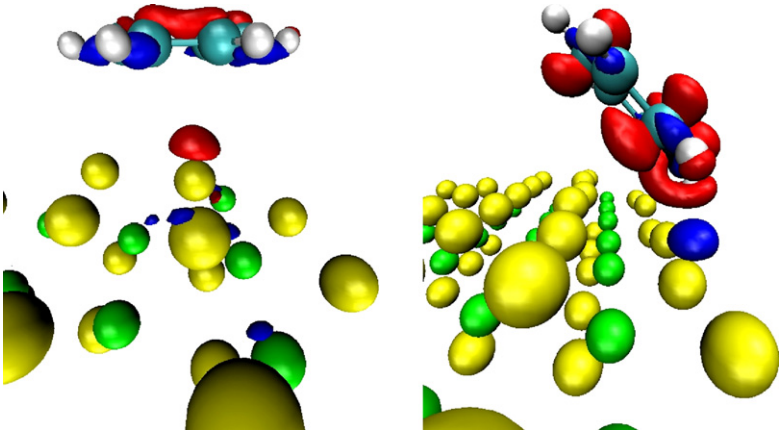

Fig. 6. Electron density difference plot of benzene (left) and pyridinium (right) on the Mo-edge. Note that in the pyridinium (left) plot, a proton has been transferred from the Mo-edge to the pyridine molecule to form a pyridinium ion. Color code: Depletion of electron density (red) plotted at a contour value of -0.03 eV/Å^3 and increase of electron density (blue) plotted at a contour value of $+0.03$ eV/Å^3. Color code of the atoms: sulfur (yellow), molybdenum (green), nitrogen (black), carbon (blue), hydrogen (white). Adapted from Ref. [97]. (For interpretation of the references to colour in this figure legend, the reader is referred to the web version of the article.)

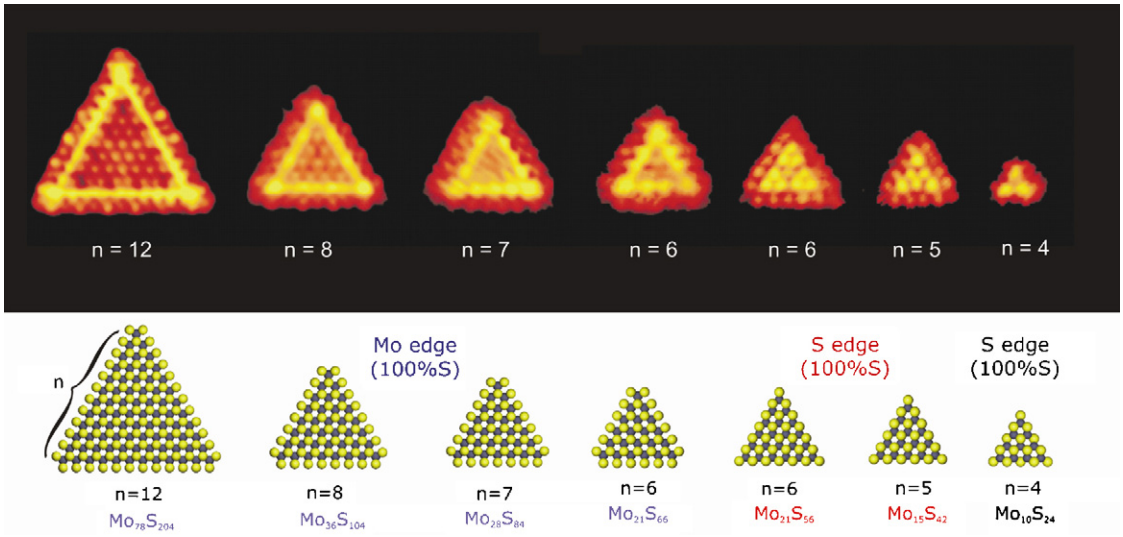

Fig. 7. STM images illustrating the structural progression of single-layer MoS_2 nanocrystals as a function of size. Upper part: STM images of cluster with varying size, where n denotes the number of Mo atoms on the cluster edge. Lower part: Ball models (top view) associated with the MoS_2 triangles observed by STM and the corresponding cluster composition Mo_XS_Y (Mo: blue; S: yellow). Adapted from [26]. (For interpretation of the references to colour in this figure legend, the reader is referred to the web version of the article.)

being the active site for the HYD pathway, and the results support that the brim sites seem to play a special role.

5. Size effects

It is well-known that materials scaled down to particles in the nanometer regime may adopt new and interesting structural and electronic properties that are significantly different from those observed in bulk systems [98]. Numerous studies have shown that this also may lead to unique catalytic properties. For example, catalysts based on gold nanoparticles supported on a metal oxide have indeed been shown to exhibit interesting size-dependent activities for low temperature oxidation reactions [99]. In a ''nanocatalysis'' context this is often highlighted as a prototype system since bulk gold is noble and catalytically inert. We have recently revealed that very strong structure-size effects also exist for MoS_2 nanoclusters catalysts, and such effects are expected to influence the hydrogenation and hydrodesulfurization activities of MoS_2 nanoclusters in this size regime [26]. Fig. 7 shows a series of atom-resolved STM images of seven single-layer MoS_2 nanoclusters with varying size. It should be noted that all clusters with the same size exhibit similar images. The large variation in the images of different size clusters demonstrates that for each cluster size there appears to be a ''unique'' minimum energy structure. The STM images also provide information on how the electronic structure like the brim sites vary with changing cluster size, and the results clearly show that the smallest clusters do not possess extended metallic states. The four largest clusters all adopt the structure described in Section 2 and in the previous studies [19,30], and these clusters are terminated by fully sulfided Mo edges. For the triangular clusters with less than six Mo atoms on the edge ($n \leq 6$), the edge structure appears differently and also the appearance of the interior of the cluster becomes brighter and different from that of normal basal planes. In Ref. [26], the structural changes were suggested to be caused by a rearrangement of the cluster edges in response to an increase of the S:Mo ratio for the smallest nanoclusters. Even in the fairly large nanoclusters ($n = 8$), a large ''excess'' of sulfur exists (S:Mo ≈ 2.89 for $n = 8$). If the edge structure remains constant, smaller clusters would have S:Mo ratios greater than three. In Ref. [26], it was noted that the large excess of sulfur can be avoided by exposing different edges (see ball models in Fig. 7). Thus, it was suggested in Ref. [26] that below a given cluster size a complete inversion of the edge structure may take place. Furthermore, for very small clusters ($n \leq 4$) indications for spontaneous formation of sulfur vacancies were noted [26] and the edge structure may be described as a ~75% S covered S edge. Importantly, this scenario illustrates that the bonding energy of sulfur in the clusters and thus the tendency to form the catalytically important sulfur vacancies on the cluster edges could exhibit a significant variation with cluster size. A detailed analysis of the images and a deconvolution of the structural and electronic effects await a full DFT-STM study. Nevertheless, even without a detailed interpretation, the present results clearly show that small MoS_2 clusters have interesting new structural and electronic properties. In view of the discussion in the previous sections, such clusters will undoubtedly also exhibit novel and very different catalytic properties and it will be an interesting challenge to prepare and investigate systems containing such clusters with well-defined sizes.

6. Conclusions and outlook

Using a combination of novel experimental and theoretical techniques like STM, DFT and HAADF-STEM, we have recently gained further insight into structure, support, size and reactivity effects in hydrotreating catalysis. One picture which emerges from these studies is the important concept of the special ''brim sites'', which we have shown to exhibit catalytic

activity for hydrogenation reactions. This is quite contrary to the common belief that vacancy sites are the key active sites, since the brim sites are not coordinatively unsaturated sites. Nevertheless, the emerging picture is shown to be consistent with many inhibition steric and poisoning effects which have been difficult to interpret using a ''vacancy model''. DFT calculations have helped us gain detailed insight into the HDS of thiophene under industrial conditions, and it is suggested that the hydrogenation reactions take place on the brim sites, whereas the sulfur removal can take place at both edges. Furthermore, the results reveal how the promoters Co and Ni change the morphology of the nanoparticles, and recently several novel forms of the Ni–Mo–S and Co–Mo–S type structures have been observed. Using STM, also unique size dependent structures of MoS_2 have been observed and these changes also result in significant variations in the electronic structure of the clusters. In the future, the new experimental and theoretical tools should be able to provide further insight into the structure sensitivity and size effects and the studies should be able to reveal how structural and morphological changes give rise to changes in the catalytic activity.

References

[1] H. Topsøe, B.S. Clausen, F.E. Massoth, in: J.R. Anderson, M. Boudart (Eds.), Hydrotreating Catalysis—Science and Technology, vol. 11, Springer Verlag, Berlin, 1996.
[2] M.V. Landau, Catal. Today 36 (1997) 393.
[3] B.C. Gates, H. Topsøe, Polyhedron 16 (1997) 3213.
[4] D.D. Whitehurst, T. Isoda, I. Mochida, Adv. Catal. 42 (1998) 345.
[5] K.G. Knudsen, B.C. Cooper, H. Topsøe, Appl. Catal. A 189 (1999) 205.
[6] T. Kabe, A. Ishihara, W. Qian, Hydrodesulfurization and Hydrogenation, Chemistry and Engineering, Wiley-CH, Kodanska, 1999.
[7] S.F. Venner, Hydrocarbon Process. 79 (2000) 51.
[8] C. Song, Catal. Today 86 (2003) 211.
[9] I.V. Babich, J.A. Moulijn, Fuel 82 (2003) 607.
[10] M. Breysse, G. Diega-Mariadassou, S. Pessayre, C. Geantet, M. Vrinat, G. Perot, M. Lemaire, Catal. Today 84 (2003) 129.
[11] M. Nagai, T. Kabe, J. Catal. 81 (1983) 440.
[12] V. LaVopa, C.N. Satterfield, J. Catal. 110 (1988) 375.
[13] P. Zeuthen, K.G. Knudsen, D.D. Whitehurst, Catal. Today 65 (2001) 307.
[14] H. Topsøe, B.S. Clausen, R. Candia, C. Wivel, S. Mørup, J. Catal. 68 (1981) 433.
[15] C. Wivel, R. Candia, B.S. Clausen, S. Mørup, H. Topsøe, J. Catal. 68 (1981) 453.
[16] B.S. Clausen, H. Topsøe, R. Candia, J. Villadsen, B. Lengeler, J. Als-Nielsen, F. Christensen, J. Phys. Chem. 85 (1981) 3868.
[17] N.-Y. Topsøe, H. Topsøe, J. Catal. 84 (1983) 386.
[18] M. Breysse, B.A. Bennett, D. Chadwick, M. Vrinat, Bull. Soc. Chim. Belg. 90 (1981) 1271.
[19] S. Helveg, J.V. Lauritsen, E. Lægsgaard, I. Stensgaard, J.K. Nørskov, B.S. Clausen, H. Topsøe, F. Besenbacher, Phys. Rev. Lett. 84 (2000) 951.
[20] J.V. Lauritsen, S. Helveg, E. Lægsgaard, I. Stensgaard, B.S. Clausen, H. Topsøe, F. Besenbacher, J. Catal. 197 (2001) 1.
[21] J.V. Lauritsen, J. Kibsgaard, G.H. Olesen, P.G. Moses, B. Hinnemann, S. Helveg, J.K. Nørskov, B.S. Clausen, H. Topsøe, E. Lægsgaard, F. Besenbacher, J. Catal. 249 (2007) 220.
[22] A. Carlsson, M. Brorson, H. Topsøe, J. Catal. 227 (2004) 530.
[23] A. Carlsson, M. Brorson, H. Topsøe, J. Microsc. 223 (2006) 179.
[24] M. Brorson, A. Carlsson, H. Topsøe, Catal. Today 123 (2007) 31.
[25] J. Kibsgaard, J.V. Lauritsen, E. Lægsgaard, B.S. Clausen, H. Topsøe, F. Besenbacher, J. Am. Chem. Soc. 128 (2006) 13950.
[26] J.V. Lauritsen, J. Kibsgaard, S. Helveg, H. Topsøe, B.S. Clausen, F. Besenbacher, Nat. Nanotechnology 2 (2007) 53.
[27] L.S. Byskov, B. Hammer, J.K. Nørskov, B.S. Clausen, H. Topsøe, Catal. Lett. 47 (1997) 177.
[28] L.S. Byskov, J.K. Nørskov, B.S. Clausen, H. Topsøe, J. Catal. 187 (1999) 109.
[29] L.S. Byskov, J.K. Nørskov, B.S. Clausen, H. Topsøe, Catal. Lett. 64 (2000) 95.
[30] M.V. Bollinger, J.V. Lauritsen, K.W. Jacobsen, J.K. Nørskov, S. Helveg, F. Besenbacher, Phys. Rev. Lett. 87 (2001) 196803.
[31] J.V. Lauritsen, M. Nyberg, R.T. Vang, M.V. Bollinger, B.S. Clausen, H. Topsøe, K.W. Jacobsen, E. Lægsgaard, J.K. Nørskov, F. Besenbacher, Nanotechnology 14 (2003) 385.
[32] J.V. Lauritsen, M. Nyberg, J.K. Nørskov, B.S. Clausen, H. Topsøe, E. Lægsgaard, F. Besenbacher, J. Catal. 224 (2004) 94.
[33] J.V. Lauritsen, M.V. Bollinger, E. Lægsgaard, K.W. Jacobsen, J.K. Nørskov, B.S. Clausen, H. Topsøe, F. Besenbacher, J. Catal. 221 (2004) 510.
[34] P. Raybaud, J. Hafner, G. Kresse, S. Kasztelan, H. Toulhoat, J. Catal 189 (2000) 129.
[35] P. Raybaud, J. Hafner, G. Kresse, S. Kasztelan, H. Toulhoat, J. Catal. 190 (2000) 128.
[36] H. Schweiger, P. Raybaud, H. Toulhoat, J. Catal. 212 (2002) 33.
[37] S. Cristol, J.-F. Paul, E. Payen, D. Bougeard, S. Clémendot, F. Hutschka, J. Phys. Chem. B 104 (2000) 11220.
[38] M.V. Bollinger, K.W. Jacobsen, J.K. Nørskov, Phys. Rev. B 67 (2003) 085410.
[39] M.Y. Sun, A.E. Nelson, J. Adjaye, J. Catal. 233 (2005) 411.
[40] P. Faye, E. Payen, A. Datta, J. Catal. 179 (1998) 560.
[41] A. Ionescu, A. Allouche, A.-P. Aycard, M. Rajzmann, R. LeGall, J. Phys. Chem. B 107 (2003) 8490.
[42] B. Hinnemann, J.K. Nørskov, H. Topsøe, J. Phys. Chem. B 109 (2005) 2245.
[43] C. Arrouvel, M. Breysse, H. Toulhoat, P. Raybaud, J. Catal. 232 (2005) 161.
[44] D. Costa, C. Arrouvel, M. Breysse, H. Toulhoat, P. Raybaud, J. Catal. 246 (2007) 325.
[45] P.G. Moses, B. Hinnemann, H. Topsøe, J.K. Nørskov, J. Catal. 248 (2007) 188.
[46] P. Raybaud, J. Hafner, G. Kresse, H. Toulhoat, Stud. Surf. Sci. Catal. 127 (1999) 327 (Hydrotreatment and Hydrocracking of Oil Fractions).
[47] S. Cristol, J.-F. Paul, E. Payen, D. Bougeard, J. Hafner, F. Hutschka, Stud. Surf. Sci. Catal. 127 (1999) 327 (Hydrotreatment and Hydrocracking of Oil Fractions).
[48] S. Cristol, J.-F. Paul, E. Payen, D. Bougeard, F. Hutschka, S. Clemendot, J. Catal. 224 (2004) 138.
[49] T. Todorova, R. Prins, T. Weber, J. Catal. 236 (2005) 190.
[50] R.R. Chianelli, M. Daage, M.J. Ledoux, Adv. Catal. 40 (1994) 177.
[51] M.W.J. Craje, S.P.A. Louwers, V.H.J. de Beer, R. Prins, A.M. van der Kraan, J. Phys. Chem. 96 (1992) 5445.
[52] A.M. de Jong, V.H.J. de Beer, J.A.R. van Veen, J.W. Niemantsverdriet, J. Vac. Sci. Tech. A 15 (1997) 1592.
[53] R.G. Leliveld, A.J. van Dillen, J.W. Geus, D.C. Koningsberger, J. Catal. 175 (1998) 108.
[54] R. Prins, V.H.J. de Beer, G.A. Somorjai, Catal. Rev. Sci. Eng. 31 (1989) 1.
[55] R. Prins, Adv. Catal. 46 (2002) 399.
[56] B.S. Clausen, B. Lengeler, R. Candia, J. Als-Nielsen, H. Topsøe, Bull. Soc. Chim. Belg. 90 (1981) 1249.
[57] J.T. Miller, C.L. Marshall, A.J. Kropf, J. Catal. 202 (2001) 89.
[58] J.V. Sanders, Phys. Scr. 14 (1978–1979) 141.
[59] J.M. Thomas, G.R. Millward, L.A. Bursell, Philos. Trans. R. Soc. A 300 (1981) 43.
[60] R. Candia, O. Sørensen, J. Villadsen, N.-Y. Topsøe, B.S. Clausen, H. Topsøe, Bull. Soc. Chem. Belg. 93 (1984) 763.
[61] F. Delannay, Appl. Catal. 16 (1985) 135.
[62] T.F. Hayden, J.A. Dumesic, J. Catal. 103 (1987) 366.
[63] J. Ramirez, S. Fuentes, G. Diaz, M. Vrinat, M. Breysse, M. Lacroix, Appl. Catal. 52 (1989) 6501.

[64] E. Payen, S. Kasztelan, S. Houssenbay, R. Szymanski, J. Grimblot, J. Phys. Chem. 93 (1989) 6501.
[65] S. Srinivasan, A.K. Datye, C.H.F. Peden, J. Catal. 137 (1992) 513.
[66] S. Eijsbouts, J.J.L. Heinerman, H.J.W. Elzerman, Appl. Catal. A 105 (1993) 53.
[67] P.L. Hansen, H. Topsøe, J.O. Halm, in: Proceedings of the 13th International Conference on Electron Microscopy, vol. 2B, Paris, (1994), p. 1077.
[68] R.M. Stockmann, H.W. Zandbergen, A.D. van Langeveld, J.A. Moulijn, J. Mol. Catal. A 102 (1995) 147.
[69] S. Eijsbouts, Appl. Catal. A 158 (1997) 53.
[70] Y. Sakushita, T. Yoneda, J. Catal. 185 (1999) 487.
[71] H.R. Reinhoudt, A.D. van Langeveld, P.J. Kooyman, R.M. Stockmann, R. Prins, H.W. Zandbergen, J.A. Moulijn, J. Catal. 179 (1998) 443.
[72] P.J. Kooyman, E.J.M. Hensen, A.M. de Jong, J.W. Niemantsverdriet, J.A.R. van Veen, Catal. Lett. 74 (2001) 49.
[73] R. Candia, J. Villadsen, N.-Y. Topsøe, B.S. Clausen, H. Topsøe, Bull. Soc. Chim. Belg. 93 (1984) 763.
[74] R.G. Leliveld, A.J. van Dillen, J.W. Geus, D.C. Koningsberger, J. Catal. 165 (1997) 184.
[75] N.-Y. Topsøe, H. Topsøe, J. Catal. 139 (1993) 631.
[76] E.G. Derouane, E. Pedersen, B.S. Clausen, Z. Gabelica, R. Candia, H. Topsøe, J. Catal. 99 (1986) 253.
[77] E.J.M. Hensen, V.H.J. De Beer, J.A.R. van Veen, R.A. van Santen, Catal. Lett. 84 (2002) 59.
[78] E. Diemann, Th. Weber, A. Müller, J. Catal. 148 (1994) 288.
[79] H. Topsøe, R. Candia, N.-Y. Topsøe, B.S. Clausen, Bull. Soc. Chim. Belg. 93 (1984) 783.
[80] J.A.R. van Veen, E. Gerkema, A.M. van der Kraan, A. Knoester, J. Chem. Soc. Chem. Commun. (1987) 1684.
[81] L. Coulier, G. Kishan, J.A.R. van Veen, J.W. Niemantsverdriet, J. Phys. Chem. B 106 (2002) 5897.
[82] M. Sun, D. Nicosia, R. Prins, Catal. Today 86 (2003) 173.
[83] X. Krokidis, P. Raybaud, A.-E. Gobichon, B. Rebours, P. Euzen, H. Toulhoat, J. Phys. Chem. B 105 (2001) 5121.
[84] C. Wolverton, K.C. Hass, Phys. Rev. B 63 (2001) 024102.
[85] G. Paglia, A.L. Rohl, C.E. Buckley, J.D. Gale, Phys. Rev. B 71 (2005) 224115.
[86] M. Digne, P. Sautet, P. Raybaud, P. Euzen, H. Toulhoat, J. Catal. 211 (2002) 1.
[87] M. Digne, P. Sautet, P. Raybaud, P. Euzen, H. Toulhoat, J. Catal. 226 (2004) 54.
[88] H. Topsøe, B.S. Clausen, Catal. Rev. Sci. Eng. 26 (1984) 395.
[89] J.C. Duchet, E.M. van Oers, V.H.J. de Beer, R. Prins, J. Catal. 80 (1983) 386.
[90] J.P.R. Vissers, B. Scheffer, V.H.J. de Beer, J.A. Moulijn, R. Prins, J. Catal. 105 (1987) 277.
[91] S. Cristol, J.F. Paul, E. Payen, D. Bougeard, S. Clémendot, F. Hutschka, J. Phys. Chem. B 106 (2002) 5659.
[92] M. Egorova, R. Prins, J. Catal. 225 (2004) 417.
[93] T.C. Ho, J. Catal. 219 (2003) 442.
[94] M. Egorova, R. Prins, J. Catal. 224 (2003) 278.
[95] N.-Y. Topsøe, H. Topsøe, J. Catal. 139 (1993) 641.
[96] M. Nagai, T. Sato, A. Aiba, J. Catal. 97 (1986) 52.
[97] Á. Logadóttir, P.G. Moses, B. Hinnemann, N.-Y. Topsøe, K.G. Knudsen, H. Topsøe, J.K. Nørskov, Catal. Today 111 (2006) 44.
[98] U. Heiz, U. Landman (Eds.), Nanocatalysis, Springer, Berlin, 2007.
[99] M. Valden, X. Lai, D.W. Goodman, Science 281 (1998) 1647.